SCIN[TAX]

Project no.:	**033 427**
Project acronym:	**ScinTax**
Project title:	**Novel Ceramic Thin Film Based Scintillator for High Resolution X-Ray Imaging**
Instrument:	**STREP**
Thematic Priority:	**NMP**

FINAL ACTIVITY REPORT

Period covered:	**October 1st 2006 to 31st October 2009**
Date of preparation:	
Start date of project:	**1st October 2006**
Duration:	**36 month**
Project coordinator name:	**Prof. Dr. Tilo Baumbach**
Project coordinator:	**Forschungszentrum Karlsruhe GmbH**
Revision:	[final_march 2010]

Summary Report

Angelica Cecilia[1]; Tilo Baumbach[1]; Olaf Jedicke[1]; Alexander Rack[2]; Thierry Martin[2]; Klaus Dupré[3]; Jonathan Murrell[4]; Jorgen Rheinlaender[5]; Xavier Rochet[6]; Uwe Zscherpel[7]; Daniel Fratscher[7]

[1] *Forschungszentrum Karlsruhe* – ANKA (Acronym FZK, Germany)
[2] *European Synchrotron Radiation Facility* (Acronym ESRF, France)
[3] *FEE GmbH* (Acronym FEE, Germany)
[4] *Photonic Science Ltd.* (Acronym PSL, United Kingdom)
[5] *Innospexion* (Acronym INOSPX, Denmark)
[6] *Optique Peter – Optical and mechanical Engineering* (Acronym OP, France);
[7] *Bundesanstalt für Materialforschung und -prüfung* (Federal Institute for Materials Research and Testing, Acronym BAM, Germany),
[8] *Central Atomic Energie - LETI* (Acronym CEA-Leti, France)

Content

1. Introduction

The project SCINTAX aimed at developing novel thin scintillating films for the application in high performance X-ray imaging and subsequent to introduce new X-ray detectors to the market for scientific and industrial applications. To achieve those aims lutetium orthosilicate Lu_2SiO_5 (LSO) scintillators doped with different activators were grown by liquid phase epitaxy (LPE) on a dedicated substrate. The LSO high density (7.4 g/cm^3) the effective atomic number (65.2) and the high light yield make this scintillator highly applicable for indirect X-ray detection in which the ionising radiation is converted into visible light and then counted by a digital detector [1, 2]. As it will be described in the following sections, the developed novel scintillating film was used in detector systems for high resolution X-ray imaging in 2D and 3D, preferably at synchrotron radiation sources. A second dedicated detector with high efficiency was built and mounted into a demonstrator also developed in the project for industrial application. The fully functionality system for X-ray online inspection will be presented for fires and exhibitions.

The ScinTAX project involved nine different partners having different competences in the X-ray imaging field: detector optimisation, certification of the achieved performance, development of the growth technique and integration of the new scintillating screens into the fully working device. The long term experience of the involved partners guaranteed the outstanding results of the project and allowed the successful accomplishment of the initially established targets.

In detail the project involved the following partners:

- *Forschungszentrum Karlsruhe* – ANKA (FZK, Germany)[1],
- *Bundesanstalt für Materialforschung und -prüfung* (Federal Institute for Materials Research and Testing – BAM, Germany),
- *European Synchrotron Radiation Facility* (ESRF, France),
- *Optique Peter – Optical and mechanical Engineering* (OP, France);
- *FEE GmbH* (FEE, Germany),
- *Innospexion* (INOSPX, Denmark),
- *Photonic Science Ltd.* (PSL, UK),
- *Central Atomic Energie - LETI* (CEA LETI, France).

The project was coordinated by the Forschungszentrum Karlsruhe GmbH.
The coordinator contact was:
Prof. Dr. Tilo Baumbach
Institute for Synchrotron Radiation
Karlsruher Institut für Technologie
D-76021 Karlsruhe Germany
Phone +49 7247 82 6820
Fax +49 7247 82 6820

Email: tilo.baumbach@kit.edu
Since January 2008 a project website was activated: http://www.scintax.eu

[1] Now *Karlsruher Institut für Technologie-Campus Süd.*

2. Scintillator requirements for high resolution applications

The basic requirements for high-resolution X-ray imaging are [3]:

—High X-ray absorption: to maximize the X-ray stopping power by coupling a high density (>5 g/cm^3) with a large atomic number (>50).

—Light emission: high conversion efficiency (>20 visible light photons/keV), emission wavelength well matched to the CCD read out (550 – 650 nm) and low afterglow (<4 decades of magnitude after 2 ms) and high linearity of the light output with the X-ray flux.

—Optical properties: high transmittance and no scattering.

—Technical aspects: machining, non-toxicity, radiation hardness and mechanical strength.

—Thickness available from 1 to 500 µm.

The LSO scintillator was chosen because of its high density (7.4 g/cm^3) and high effective atomic number (65.2). Its absorption gain compared to a standard $Y_3Al_5O_{12}$:Ce (YAG) scintillator can be as high as a factor of 2.4 below 10 keV, 10.5 between 10 keV and 17 keV, 2.2 between 17 keV and 63 keV and from 63 keV to 100 keV. In Figure 1 we have reported the theoretical absorption efficiencies of a 5 µm LSO in comparison with the YAG and the $Lu_3Al_5O_{12}$Ce:Ce (LAG) LAG scintillators commonly used in synchrotron applications. In addition, the experimentally measured LSO:Tb absorption efficiency is reported in the energy range between 20 keV and 60 keV [3].

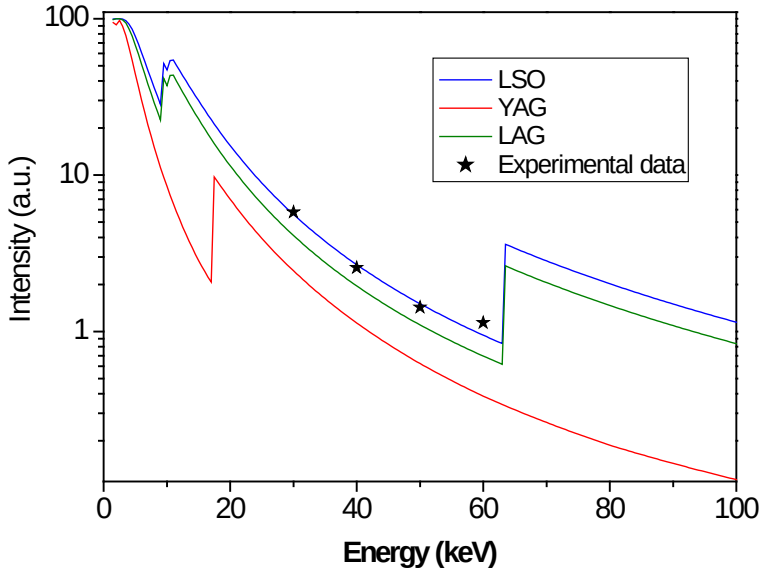

Figure 1: Absorption efficiency of 5 µm thick SCFs as function of the X-ray energy (calculated for LSO, LAG, and YAG; experimentally verified for LSO).

3. Growth of scintillating LSO layers by Liquid Phase Epitaxy technique

The liquid phase epitaxy is a technique for growing single crystal layers on oriented single crystal substrates. Both the substrate and the epi-layer growths were developed and demonstrated by CEA/LETI during the 1st year of project. The initially chosen Y_2SiO_5 (YSO) substrate was found not perfectly fitting the LSO LPE and the choice went onto another material [4]. High grade quality substrate were grown by the Czochralski pulling technique and representative sample were provided to ESRF and FZK to be characterised in terms of radiation damage, X-ray fluorescence and to verify the possible presence of unwanted substrate radioluminescence. Very often the substrates used to deposit the scintillating films emit undesired luminescence and such effect could deteriorate the spatial resolution performance reachable with the later scintillating film [5, 6]. The radiation damage turned out to be a reversible process and the analysis of the X-ray fluorescence spectra evidenced a presence of impurities with concentration below 1 %. As reported in [7] the substrate radio-luminescence spectrum is completely free from any parasitic component. The absence of luminescence from the substrate strongly improves the spatial resolution of the X-ray images, especially for film thickness below 20 µm and at high X-ray energies above 20 keV, at which only a small part of the X-rays are absorbed in the thin films. This effect is clearly illustrated in the Figure 2, showing an increased contrast when a LSO:Tb thin film is used.

Figure 2 : Radiographs of a powder injection moulded micro-part [8] obtained at the ID19 beamline (ESRF) using a) LAG:Eu/YAG 10µm SCF, b) GGG:Eu/GGG 6.2µm SCF, c) LSO:Tb/YbSO 10µm SCF. The X-ray energy used is 27keV. Specimens courtesy of O.Weber, funded by DFG, SFB499.

Different dopants were tested to optically activate the LSO crystal matrices. Solely Eu^{3+}, Tm^{3+} and Tb^{3+} could be added as main dopants in the LSO lattice. For other dopants (e.g. Ce^{3+}, Pr^{3+}), the lattice mismatch between the substrate used and the film was too high or the segregation coefficient was to low, resulting in the growth of bad optical quality layers. Tb rare earth ion was finally chosen because it is the only rare earth ion that can be properly adjusted both to fit the substrate lattice parameters and to provide a very high conversion efficiency for a range of dopant concentration (up to 130% YAG:Ce light yield). In addition its green emission (Figure 3) is efficiently detected by the front-illuminated CCD cameras commonly used in the synchrotron community (Figure 4). Ce co-doping of LSO layers with Tb ions turned out to be also efficient. The ion adds a contribution peaked at 420 nm in the emission spectrum (without quenching the emission due to Tb).

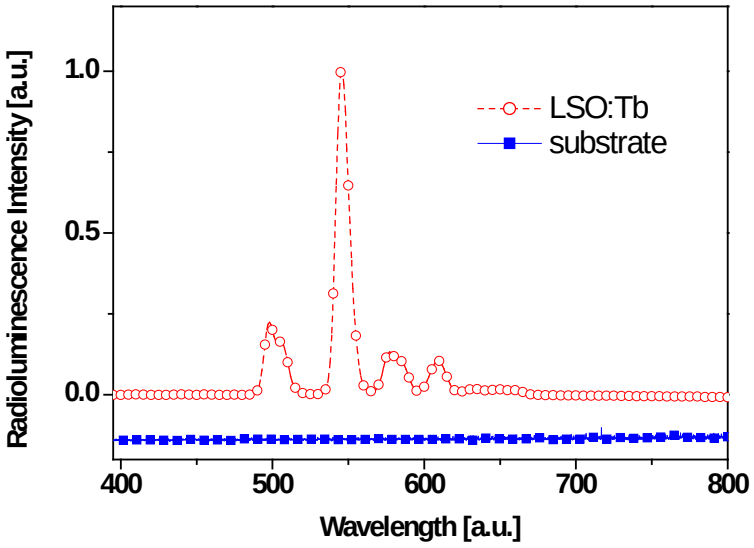

Figure 3: Radio-luminescence spectra of LSO:Tb^{3+} and of substrate.

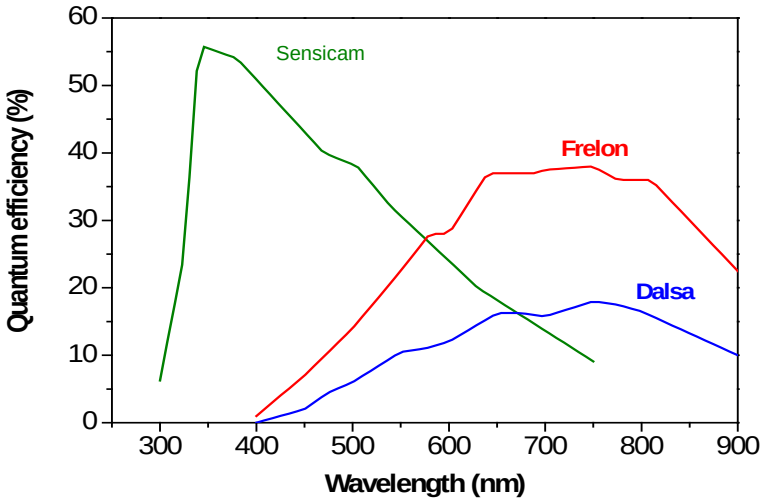

Figure 4: Quantum efficiency (QE) comparison of fast CCD cameras (FReLoN 2 k14 bit, Dalsa 1M60) is in the red region while interline-transfer CCD cameras (e.g., Sensicam) have commonly a QE at shorter wavelengths.

After establishing (1st year of project activity) that LSO:Tb is the most suited scintillator for the ScinTax application, the activity focused on the optimisation of Tb content. The concentration of Tb was varied from 3 to 15 atomic-% in the melt and the scintillating LSO/substrate performances were investigated vs. dopant concentration, growth rate and post-growth treatment. The best light yield values were obtained when [Tb] =15%, the growth rate is equal to 0.2 µm/min and the sample undergoes a 30 h post-growth thermal annealing at 1100 °C.

Contemporarily to optimising the growth technique, CEA/Leti started transferring the LPE technology to the FEE partner, which will manage the up-scaling production of the scintillators[2]. A facility for the growth of thin films was designed and installed at FEE, consisting mainly of a furnace where the melt is heated up in a platinum crucible, of

[2] After the 1.5 year meeting CEA/Leti left the project due to internal reorganization.

translation and rotation stages for the movement of the substrate and of control units to govern the process. Figure 5 shows a sectional drawing of the furnace (left part) and the measured thermal gradient in the furnace (right part). The thermal gradient is modulated by three ceramic shields in the upper part of the furnace and a shielding plate above the crucible. The results are a constant temperature in the melt, which is essential for the LPE and a nearly constant thermal gradient in the upper part of the furnace, which prevents thermal induced cracking of the substrate during the movements.

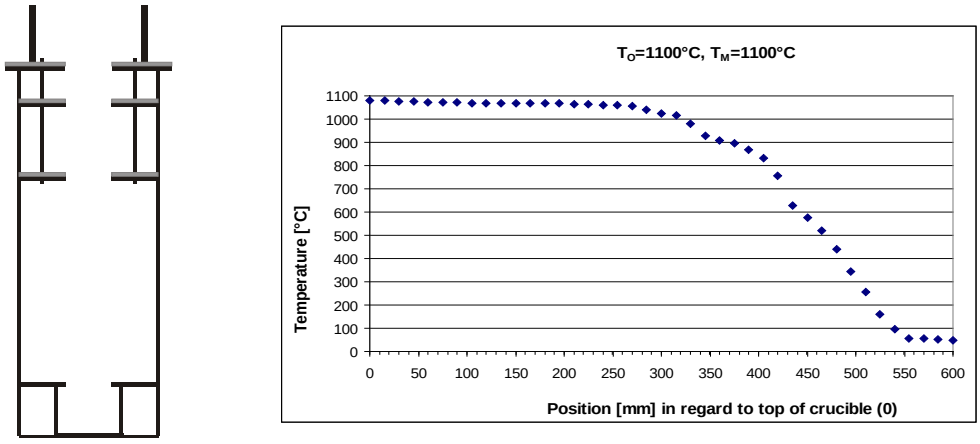

Fig.5: Sectional drawing of the furnace (left part) and measured temperature plotted against the position (right part).

For the LPE the substrate is moved in the melt. The epitaxy time is in the range of several minutes for the growth of thin layers and some hours for the growth of thick layers. To get homogeneous layers of high quality, it is necessary to keep the growth rate constant. This is a challenge for thick layers and requires a special process control. After the optimisation LSO layers were grown with a thickness of up to 110 µm, the thickest LSO layers grown so far by LPE. Attempts to grow thicker layers resulted in breaking of the crystals, probably due to a slight mismatch of the crystal lattices of the substrate and the layer, which induces stress in the crystal. FEE grew up successfully also several substrate crystal boules and accomplished a process for the polishing of the substrates (Figure 6) Manufacturing of scintillators requires grinding, polishing and cutting of the samples produced by LPE. These samples consist of the 500 µm thick substrate with doped LSO layers on both faces. One layer has to be removed and for high resolution applications, the sample must be thinned down to 170 µm where usually the cover glass correction for microscopic optics are working. For thick layers an additional polishing of the layer is necessary. The last manufacturing step is the cutting of the scintillators. The manufacturing process is a challenge because the samples have the tendency to cleave. The process works well for scintillators with thin oxide films (thickness below 20 µm), but it is problematic for scintillators with thicker layers (> 30 µm). Due to the difficulty encountered for growing thick LSO epilayers onto the optimised substrates, the epitaxial process was tested on a different material and it was proved being successful on LYSO substrates with about 500 µm thickness.

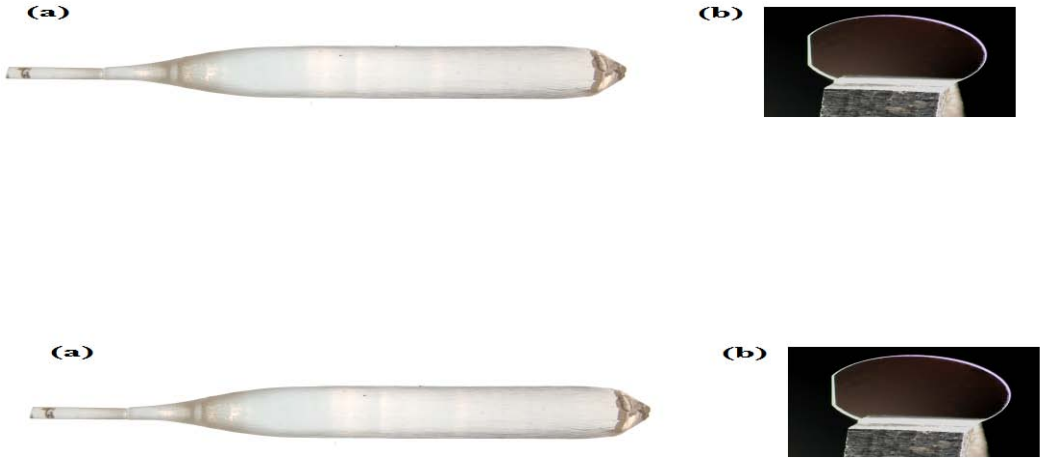

Figure 6: (a) substrate orthosilicate crystal boule (diameter: 30 mm, length: 115 mm); (b) substrate (diameter: 1 inch, thickness: 500 µm).

4. High Resolution detector

The high resolution detector manufactured during the Scintax collaboration consists of an indirect X-ray detector in which the newly developed LSO:Tb scintillating crystals are combined with diffraction limited microscope optics. The magnified light image is next recorded onto a CCD. In Figure 7(1) we have reported the typical structure of an indirect X-ray imaging detector and in Figure 7(2) the overall Scintax high resolution detector during its commissioning at the ANKA-TopoTomo beamline in November 2008.

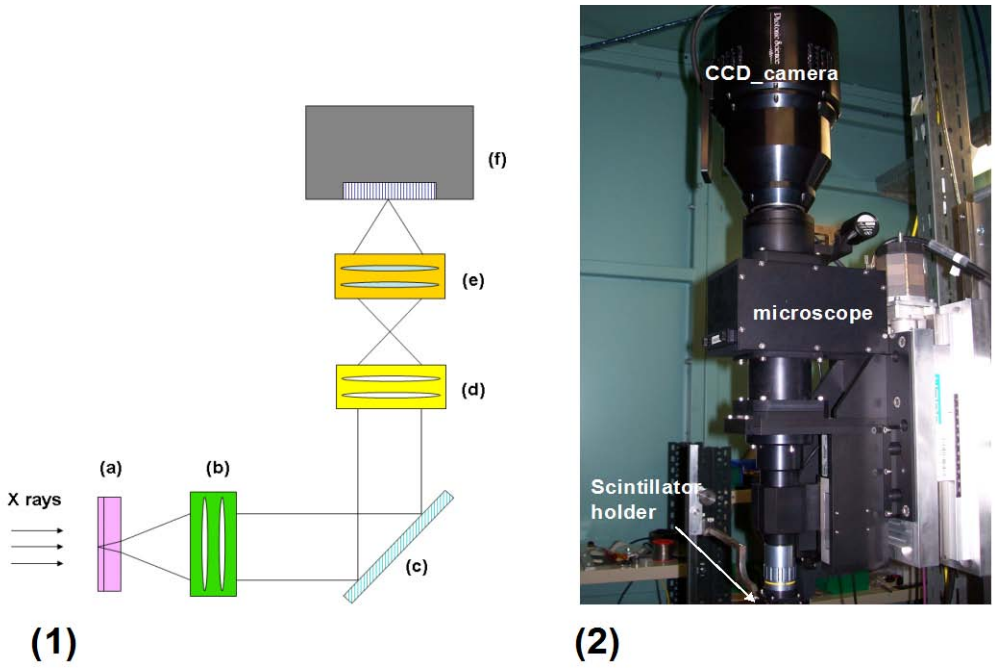

Figure 7: (1) X-ray imaging based on transparent scintillators combined with diffraction limited microscope objectives (a=scintillator; b=objective lens; c=mirror; d=tube lenses; e=photoeyepiece; f=CCD camera) [3, 9, 10]. (2) Picture of the Scintax high resolution detector

4.1 CCD detector

The CCD detector was accomplished by PSL, which developed a new board sets to allow the 11M pixel Kodak sensor to be operated in two-tap mode. During the 2nd year of project, PSL tested the single tap 10MHz high resolution prototype camera based on the Kodak KAI-16000 image sensor. The key results of the tests are a Responsivity = 6.5e/adu, a RMS noise darkness = 2.4 ADU (29 e^-) a Full Well Capacity = 27000 and a Dynamic Range = 60 dB. The linearity is lower than 2% deviation and three different frame rate are available (Bin 1: 0.98 fps, Bin 2: 1.9 fps and Bin 4: 4 fps). The detector was designed in such a way that during the last year of project the electronic hardware and firmware were updated to the 2 tap 20 MHz version without modifying the metalwork. After upgrading the 16MP 20MHz 2-tap high resolution camera, PSL carried out the test procedures. The key results of the tests are a Responsivity = 7.03 e/adu, a RMS noise darkness = 5.5 ADU (38 e-) a Full Well Capacity = 28400 e- and a Dynamic Range = 57.5 dB. The linearity is lower than 2% deviation and three different frame rates are available (Bin 1: 2.1 fps, Bin 2: 3.8 fps and Bin 4: 6.5 fps). These results, although

encouraging, show that further work would be required to achieve performance necessary for a viable commercial product. The finally delivered PSL CCD camera is reported in Figure 8.

Figure 8: High resolution CCD camera delivered by PSL

4.2 High Resolution Microscope

The microscope design was presented and approved during the 1st year meeting in Berlin (Figure 9). It was manufactured by *Optique Peter* and it consists of a modular system that can be adapted to a wide range of camera formats and interfaces. It can be used in two configurations: monochromatic and white beam/pink mode. The *Optique Peter* assembled microscope was shown to the partners during the 2nd year Scintax meeting (ESRF, Grenoble, 9-10 September 2008) and it was delivered at end of October 2008. In Table I and in Table II we have summarised the optical data of the monochromatic and white beam/pink microscope configuration in combination with large sensor camera.

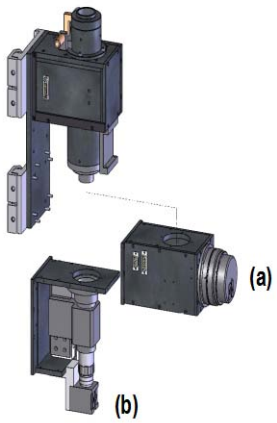

Figure 9: Optique Peter microscope

Figure 10: Optique Peter microscope. (a) Monochromatic setting; (b) White beam setting

Table I: Monchromatic beam microscope used in combination with large sensor cameras

Objective	1.25 X	2 X	4 X	10 X	20 X
NA	0.04	0.08	0.16	0.40	0.75
Working distance (mm)	5.10	6.20	13.0	3.10	0.65
Resolution limit (µm)	7.63	3.81	1.91	0.76	0.41
PSL Scintax camera - 2,5X eyepiece					
(4872x3248 pixels 7,4 x 7,4µm)					
Hor. Object field (mm)	14.4	9.0	4.5	1.80	0.90
Vert. Object field (mm)	9.6	6.0	3.0	1.20	0.60
Hor. Object pixel size (µm)	2.96	1.85	0.93	0.37	0.19
Vert. Object pixel size (µm)	2.96	1.85	0.93	0.37	0.19
PSL VHR camera - 2,5X eyepiece					
(4008x2672 pixels 9x9µm)					
Hor. Object field (mm)	14.4	9.0	4.5	1.80	0.90
Vert. Object field (mm)	9.6	6.0	3.0	1.20	0.60
Hor. Object pixel size (µm)	3.60	2.25	1.13	0.45	0.23
Vert. Object pixel size (µm)	3.60	2.25	1.13	0.45	0.23
Frelon camera - 2,5X eyepiece					
(2048x2048 pixels 14x14µm)					
Hor. Object field (mm)	11.5	7.2	3.6	1.43	0.72
Vert. Object field (mm)	11.5	7.2	3.6	1.43	0.72
Hor. Object pixel size (µm)	5.60	3.50	1.75	0.70	0.35
Vert. Object pixel size (µm)	5.60	3.50	1.75	0.70	0.35

Table II: White/pink beam microscope used in combination with large sensor cameras

- Optical data - White beam / Pink beam Microscope
- Large size sensors cameras
- Examples for PSL and Frelon cameras

Optique Peter

Long working distance objective	**2 X**	**5 X**	**5 X**	**10 X**	**10 X**	**10 X**
Eyepiece	**2,5 X**	**2.5 X**	**3.3 X**	**2.5 X**	**3.3 X**	**4 X**
Total Magnification	**5.56**	**13.89**	**18.33**	**27.78**	**36.67**	**44.44**
NA	0.055	0.14	0.14	0.28	0.28	0.28
Working distance (mm)	34	34	34	33	33	33
Resolution limit (µm)	5.55	2.18	2.18	1.09	1.09	1.09
PSL Scintax camera - 2,5X eyepiece						
(4872x3248 pixels 7,4x7,4µm)						
Hor. Object field (mm)	6.5	2.6	2.0	1.30	0.98	0.81
Vert. Object field (mm)	4.3	1.7	1.3	0.87	0.66	0.54
Hor. Object pixel size (µm)	1.33	0.53	0.40	0.27	0.20	0.17
Vert. Object pixel size (µm)	1.33	0.53	0.40	0.27	0.20	0.17
PSL VHR camera - 2,5X eyepiece						
(4008x2672 pixels 9x9µm)						
Hor. Object field (mm)	6.5	2.6	2.0	1.30	0.98	0.81
Vert. Object field (mm)	4.3	1.7	1.3	0.87	0.66	0.54
Hor. Object pixel size (µm)	1.62	0.65	0.49	0.32	0.25	0.20
Vert. Object pixel size (µm)	1.62	0.65	0.49	0.32	0.25	0.20
Frelon camera - 2,5X eyepiece						
(2048x2048 pixels 14x14µm)						
Hor. Object field (mm)	5.2	2.1	1.6	1.03	0.78	0.65
Vert. Object field (mm)	5.2	2.1	1.6	1.03	0.78	0.65
Hor. Object pixel size (µm)	2.52	1.01	0.76	0.50	0.38	0.32
Vert. Object pixel size (µm)	2.52	1.01	0.76	0.50	0.38	0.32

4.3 Characterisation of the high resolution detector at the syncrotron facilities

4.3.1 Commissioning of the white/pink microscope

During the first week of November 2008 the white/pink microscope was tested at the ANKA-TopoTomo beamline whose characteristic features are the first slit system in the front end, no optical component inside the 30 m long beam and a second in-vacuum slit system followed by only one Be window directly in front of the experiment. The available white beam energy spectrum ranges between 1.5 up to 40 keV and the flux at sample position is $1x10^{16}$ ph/s (10x $10mm^2$) [11, 12, 13]. In order to lower the X-ray flux and protect the optics a 1 mm Si filter was used with a resulting spectrum peaked at about 20 keV. The microscope was used in combination with the high resolution PSL 10MHz camera based on the Kodak KAI-16000 image sensor, whose key properties are a full well capacity of 27000 and a noise darkness of 29 e- rms providing a dynamic range of 60 dB. The pixel dimension is equal to 7.5x7.5 μm^2. In Figure 10 we have reported the view of the overall detector.

The performance of the optics was checked by acquiring the images of the X-Radia pattern test X500-200-30 and by using a 12 µm scintillating LSO:Tb film grown on suitable substrate by LPE [3]. The target test images were acquired for the objectives 2.5x, 3.3x and 4.0x, whose combination with the 10x eyepiece provide an effective magnification M_{eff}=22.5x, 29.7x and 36x and an effective pixel sizes 0.33, 0.25 and 0.21

μm for the PSL camera. The numerical aperture of each objective is equal to 0.28 and that sets the resolution limit at 1.09 μm for a scintillator emission peak at 500 nm. The distance between the target and the scintillator was equal to 22 mm. In both the configurations, the performance of the microscope turned out to be excellent as the optical system allowed resolving the target test structures up to the theoretical resolution limit of 1.1-1.2 μm for all the used magnifications. In Figure 11 we reported a representative example of such behaviour for the pixel size of 0.25 μm.

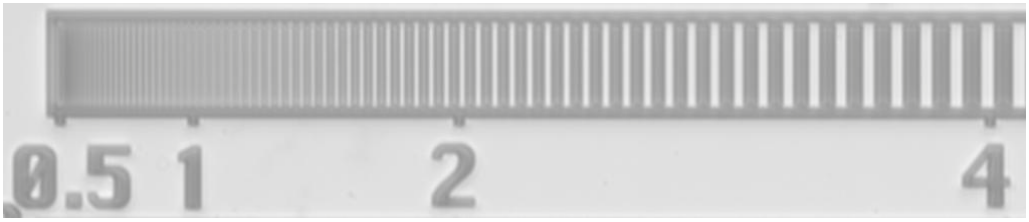

Figure 11: Vertical pattern test of the X-radia target (effective pixel size=0.25 μm, 12μm LSO:Tb scintillating film, M_{eff}=36 x).

In February 2009 the white beam microscope was commissioned under the high intense flux and hard wavelength available at the ESRF-ID15a beamline where an asymmetric multipole wiggler (AMPW) provides a white beam spectrum between 44 keV up to 500 keV [14]. During that experiment the the overall system was radiation shielded with a 3mm Pb layer and the high radiation flux was attenuated with 25 mm Si and 5 mm Cu filters. The beam had dimensions of 1x1 mm^2. The most prominent effect we observed during the commissioning was the browning of the objective due to the scattered radiation from the target and we estimated a signal intensity decrease of about 5.5 %/hour. Such effect negatively reverberates on the DQE of the overall system, due to the reduced number of photons impinging the CCD sensor. To protect the objective we added a 4 mm shielding glass before the objective and we reduced the beam size to 0.5x0.5 mm^2. Thank to those modifications the signal intensity loss was reduced by an order of magnitude up to 0.6 %/hour. Different solutions were considered from *OP* to prevent the browning of the objective: shielding of the objective and of the microscope; mirror drilling or substitution with a vitreous carbon or a tungsten mirror. The final choice was the combination of a radiation shielding for the detector and an objective protecting lead glass.

4.3.2 Commissioning of the monochromatic beam microscope

The monochromatic microscope was commissioned in March 2009 at the ESRF-BM05. That beamline serves as a test and development station for X-ray optical elements, beam characterisation and instrumentation R&D in general and it covers an energy-range from 6 keV to 60 keV. The aim of the investigation was to study the dependence of the spatial resolution on the SCF thickness and on the NA of the objective. To accomplish it, several images of an X-radia X500-200-30 test pattern were acquired at the energy of 18 keV for a set of selected SCF with thickness between 5 up to 100 μm for each objective numerical aperture (4x/NA=0.16, 10x/NA=0.4 and 20x/ NA=0.75). To compare the spatial resolution values we have calculated for each image the contrast value relatively to a pattern structure. In Figure 12 we have reported the dependence of the CTF vs.

thickness for the NA=0.16 (Figure 12a) for the NA=0.4 (Figure 12b) and the NA=0.75 (Figure 12c).

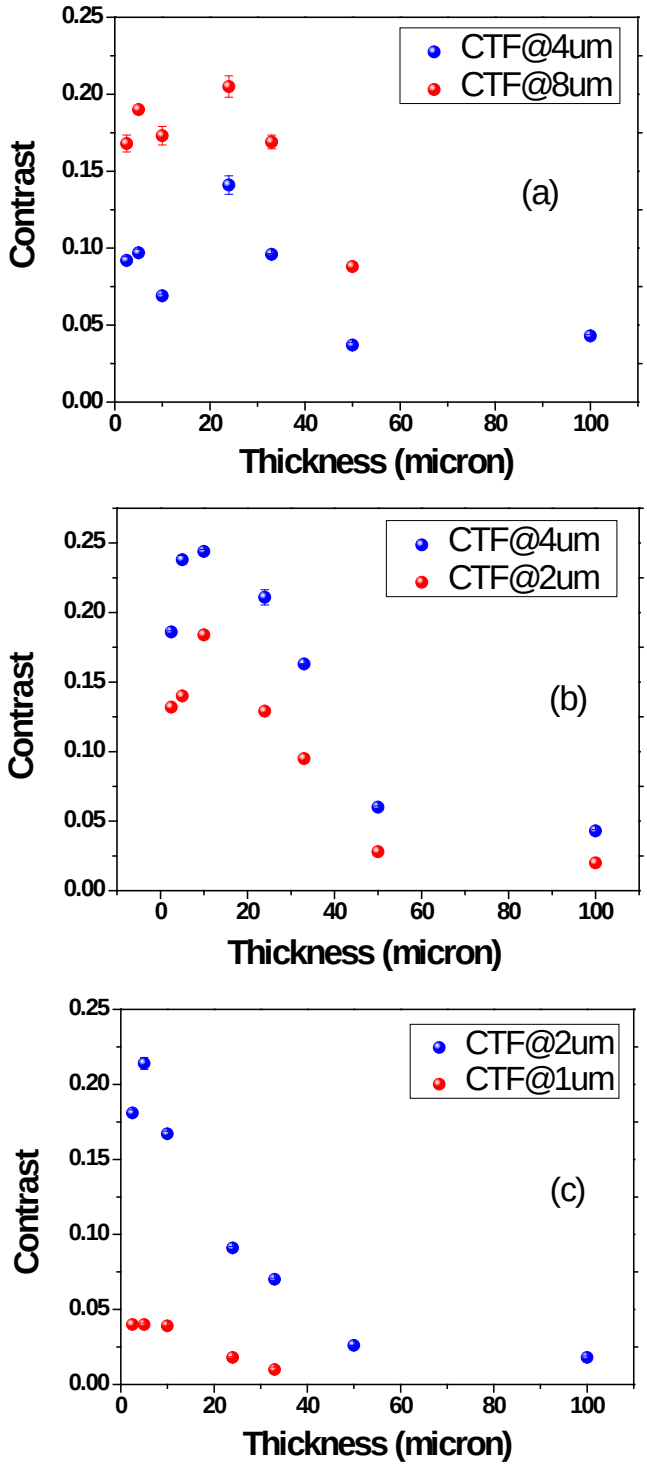

Figure 12: CTF vs. SCF thickness for the NA=0.16 (a) NA=0.4 (b) and NA=0.75 (c) at 18 keV.

The optimal LSO thickness to maximise the spatial resolution is equal to 25µm, 10µm and 5µm for the NA=0.16, 0.4, and 0.75. The obtained results are in perfect agreement

with the course of the spatial resolution versus numerical aperture NA calculated by Koch in 1998 [5] and described by the following law:

$$R = \sqrt{\left(\frac{p}{NA}\right)^2 + (qzNA)^2}$$

Where z is the thickness of the scintillator and NA the numerical aperture. *P* and *q* are fitting parameters. In Figure 13 we have reported the course of the CTF vs. thickness for the NA=0.95 measured with an ISG high resolution detector at the energy of 25 keV.

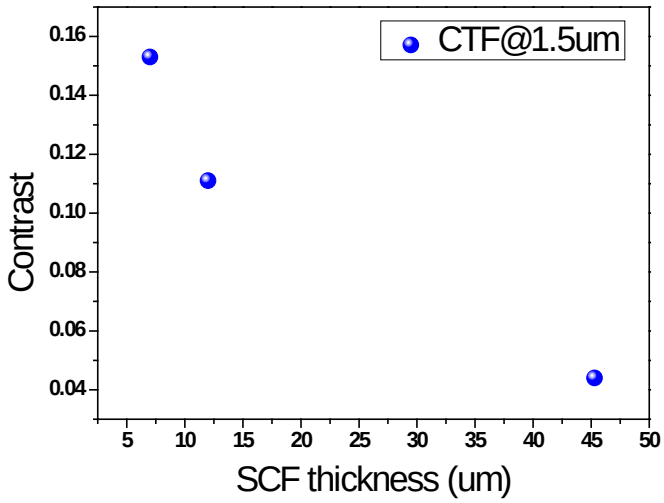

Figure 13: CTF vs. SCF thickness for the NA=0.95

The best spatial resolution value was achieved close to 0.5µm by using a 7µm LSO:Tb/substrate (Figure 14). That result is extremely promising: the optimal thickness (concerning contrast) should be smaller than 7µm. From the resolution point of view it indicates that it should be possible to get down to lower resolution by using 1-3µm thick layers.

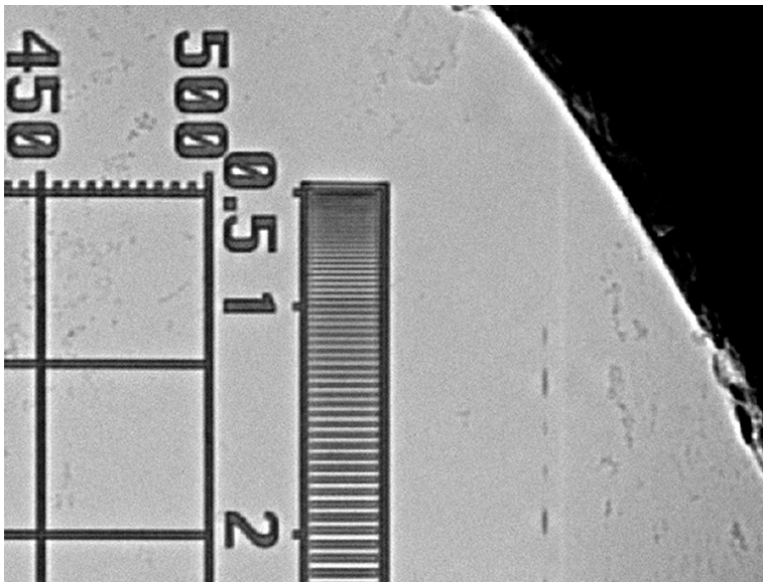

Figure 14: X-radia X500-200-30 test pattern measured at 25 keV with 40x/NA=0.95 [3]

4.3.3 Scintillating LSO:Tb efficiency measurements

The conversion efficiency of the LSO:Tb SCF was measured as a function of the x-ray energy in the range between 5-60 keV. The measurements were performed by using the FreLoN 2k and the SensicamQE CCD detectors, which are characterized by different quantum efficiency, peaked in the red and in the ultraviolet-blue spectral region respectively. In addition, the efficiency values were calculated relatively to the GGG SCF which is optimized to work coupled with the FreLoN 2k detector.
In Figure 15a we have reported the efficiency of LSO:Tb 10um compared to GGG:Eu 10um and measured with a SensicamQE CCD detector. Figure 15b shows the efficiency curve measured with the FreLoN 2k detector. As it can be seen, the efficiency increases at the LSO absorption edge at 63 keV.

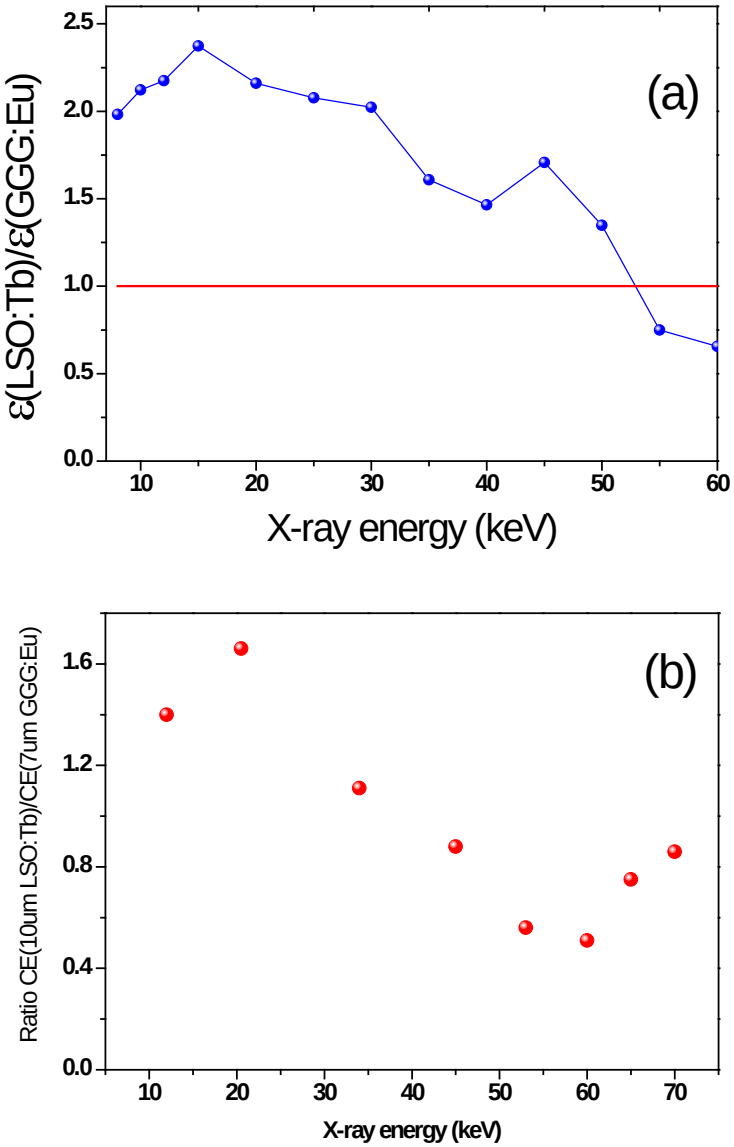

Figure 15: Efficiency of LSO:Tb compared to GGG:Eu measured with SensicamQE (a) and Frelon 2k (b)

Results evidence that the LSO:Tb/YbSO is the most efficient SCF when used with a back-illuminated or an interlined CCD chip, in the X-ray energy range between 0-51keV and between 63-100keV (Figure 15a). GGG:Eu/GGG is the most efficient in the range between 51keV-63keV. LSO:Tb/YbSO is the most efficient SCF when used with a front-illuminated frame transfer or full frame CCD chip, in the X-ray energy range between 0-20keV (Figure 15b). On the contrary GGG:Eu/GGG is the most efficient in the range [20keV;100keV].
The efficiency of the LSO:Tb scintillator turned out to not increase as fast as for other scintillators with the X-ray energy. Therefore LSO:Tb/YbSO will be preferred for X-ray applications at low X-ray energy (<30keV).

4.3.4 High spatial and temporal resolution application

Scintillating LSO:Tb/YbSO crystals with thickness lower than 25μm were tested for high-resolution tomography/radiography at the ESRF/ID19 and ID22 beamlines and the collected results were extremely good. In Figure 16 we have reported a microtomografic image, showing the feet of a honey bee (specimen courtesy of Dr M. Kuebacher, *Helmoltz-Zentrum* Berlin) and acquired using 2 μm spatial resolution at the ESRF beamline ID22.

Figure 16: Microtomografic image of a honey bee's feet.

At the ANKA/TopoTomo beamline an extraordinary fast tomography scan was performed in less than 1 second by combining a 74 μm LSO with a Rodenstock TV-Heliflex objective (f = 50 mm, max. NA = 0.43) providing an effective 3.6x magnification with Nikon (f = 180 mm tele) and with the ultrafast Photron CMOS camera (Figure 17). A complete tomography scan of a Peruphasma insect egg was

completed in 0.4 s acquisition time, with a 70% DR, 800 projections and rotation equal to 450°/sec.

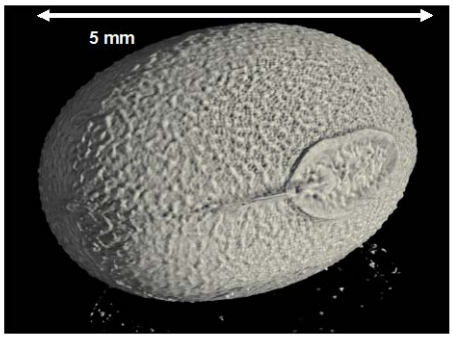

Figure 17: Microtomografic image of a Peruphasma insect egg

5. High sensitivity detector

The design for the industrial detector (Figure 18) was compiled during the 1st half year meeting. The requirement was to provide a high sensitive detector to be used in the evaluation of scintillators focused on industrial X-ray applications. The proposed arrangement placed the substrate directly on the fibre optic surface with X-rays incident side on making use of the full thickness of the substrate. The detector therefore required an adjustable collimator at the input to account for variation in scintillator depth. It also required that the detector could cope with scintillator dimensions up to 20 x 50 mm. A reducing taper was designed to de magnify the image, with the small end bonded to the CCD sensor.

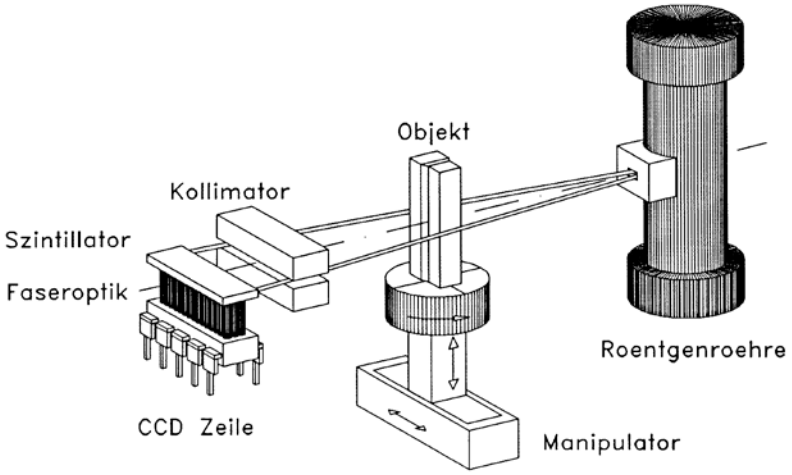

Figure 18: Sketch of the industrial detector design

5.1 CCD detector

A prototype module was developed by PSL based around the TI TX285 sensor (Figure 19) the module consisted of three main components.

1) CCD Headboard capable of driving the TI device with required clocking voltages along with readout components (analogue amplification and A to D conversion)
2) PLD board based on Altera Cyclone FPGA, used to provide CCD and data flow control as well as communication and interface control.
3) Digital Interface board based on CamerLink interface standard (Base configuration). This interface incorporates both Data and RS232 lines.

Figure 19: High sensitivity camera developed by PSL

PSL designed also the mechanical housing for the prototype boards and they performed the testing and debugging. In addition they developed the PC software and debugging together with the design of complete detector enclosure along with specification of optical components and bonding procedures. With the high energies involved, it was important that the sensor/electronics and fibre optic were sufficiently shielded from the X-Rays. The optical taper was optimised to maximise light throughput with respect to the large taper ratio (6.25:1) and the single piece optic is the result of a careful review with the taper manufacturer. A number of factors were taken into account in the specification and design of the fibre optic taper. Firstly, the input size of 50mm square and 8mm active area on the sensor required taper ratio of 6:1.CCD to taper bond was then completed ready for assembly into metalwork enclosure (Figure 20a). The 15 mm thick tungsten line collimator device was delivered by BAM and it is equipped with micrometer screws which allow adjusting the slit from 50 μm up to 100 μm (Figure 20b).

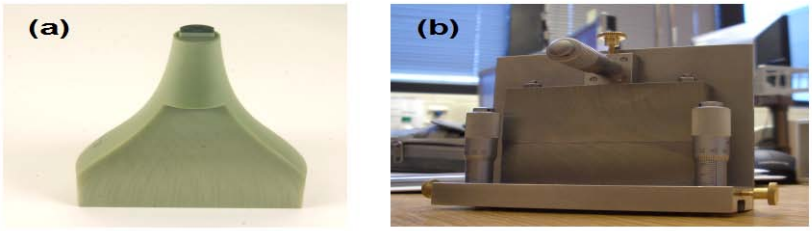

Figure 20: (a) Taper (b) Tungsten collimator of the industrial detector

5.2 X-ray cabinet

The definitive design of the demonstrator set-up was presented by INNOSPX to the partners during the 2nd year Scintax meeting. It was optimised in collaboration with PSL and the issue involved the design of a unit which is robust and which can be used both for the assessment by the partners for the evaluation and tests of the detectors in different stages of development, and later on also for the demonstration and dissemination activities (demonstrations, presentations at fairs, workshops, exhibitions, etc.). The system, shown in Figure 21, was sent to PSL by June 2008 and next it was delivered to BAM for the final optimisation.

Figure 21: The SCINTAX x-rays testing facility (complete system) for evaluation and presentation of frame mode imaging detector (The system is a stand-alone system for manual insertion of a sample at a time through a sliding door in the cabinet front. There is no detector fitted).

The used X-ray source is a ThermoKevex minifocus PXS11-150-75 X-ray source (PC controlled 75 kVp max, 9 W, 0.15 mA, air cooled). The system is fitted into a cabinet divided into two parts: the upper part is the control box comprising the X-ray controller, the computer, the electronics and the power supplies. The control box is finished in stainless steel 1.5 mm thick and it is mounted with bolts to the inspection box. The lower part of the cabinet comprises the X-ray inspection volume. This part is made radiation safe and is elaborated in 8 mm stainless steel plates, apart from the left end plate which is a sandwich structure with 2.5 mm lead. To the front is fitted a lead glass conforming to a maximum X-ray energy of 110 kV.

The software for the line detector control was completed by BAM using Labview GI and in December 2008 the operation with the line demonstrator was started. Due to the lack of high quality thick LSO scintillators, the initial tests were performed by using a structured CsI scintillator deposited on FOP (fibre optical plate, *Hamamatsu Photonics*). Some preliminary line scan radiographies were performed successfully by visualising the copper wires and the metal connections of a PC mouse PS/2 connector. In addition, a double wire IQI test pattern (W and Pt wires) was used to measure the spatial resolution.

The smallest measurable diameter in the x- direction is equal to 0.08 and in y- direction 0.05 mm. The demonstrator allows for performing of tomographic scans of a selected layer by rotating the object but further developments are required to optimise the CT algorithm.).

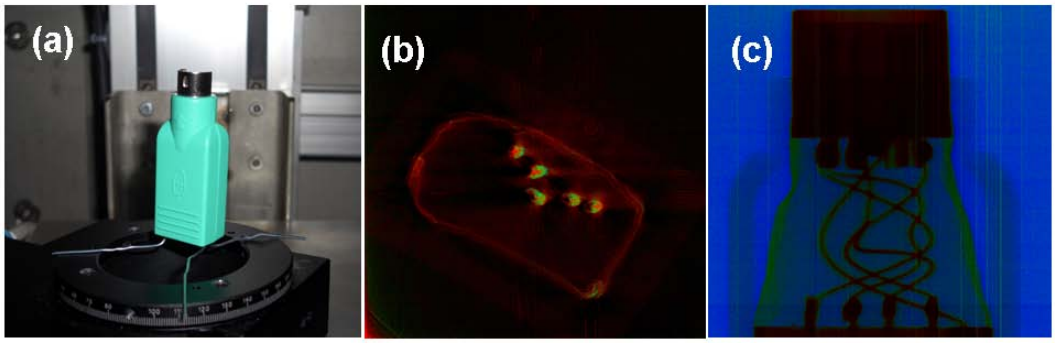

Figure 22: Image: Picture of the scanned USB mouse (a); tomographic reconstruction of a slice (b); multiple energy mode radiography of the USB mouse

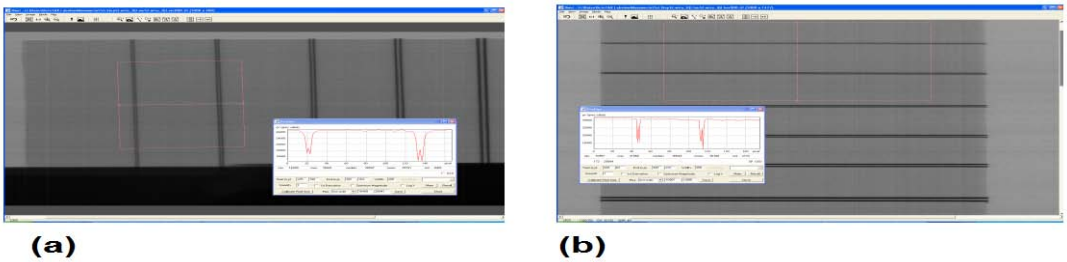

Figure 23: Spatial resolution measurement performed with a double wire IQI on the line scanning detector. (a) x- direction (b) y- direction

The line inspection system allows for a versatile use in different configuration, depending on the required application: direct irradiation (perpendicular to scintillator), high sensitivity mode, multiple energy mode. The theoretical simulations done during the project proved tha it is possible to calculate the incoming spectra, but a very high signal to noise ratio is needed, attenuation coefficients of the scintillator have to be known very well.

6. Delivered Standard and Patent

BAM finalized a Standard ASTM E2597-07 "Standard Practice for Manufacturing Characterisation of Digital Detector Arrays" and published it in January 2008. That Standard includes the description of different test methods for characterizing digital imaging devices in terms of spatial resolution (SRb duplex wire based on ASTM 2002, high spatial resolution with JIMA RT RC-0.2) SNRn and achievable contrast sensitivity.

A patent was submitted in Germany with the title "*Festkörperleuchtschirm für ortsaufgelöste Detektion ionisierender Strahlung*"and it was registered with the number 10 2007 054 700.714.11.2007. The citations from the German Patent Office were notified to K. Dupré (FEE) and 18/30 months are still available for taking decision upon the other countries.

References

[1] C. L. Melcher, J. S. Schweitzer, IEEE Trans. Nucl. Sci., vol. 39, no 4, 502-505, 1992.
[2] C. L. Melcher, M. A. Spurrier, L. Eriksson, M. Eriksson, M. Schmand, G. Givens, R. Therry, T. Homan, R. Nutt, IEEE Trans. Nucl. Sci., vol. 50, no 4, 762-766, 2003.
[3] T. Martin et al., "*LSO-based single crystal film scintillator for synchrotron-based* hard X-ray micro-imaging", IEEE Transactions on Nuclear Science vol. 56, no. 3, 1412-1418 (2009).
[4] K. Dupré, M. Couchaud, T. Martin, A. Rack, German Patent Application no. DE 10 2007 054 700.7 (2007).
[5] A. Koch, C. Raven, P. Spanne, A. Snigirev, J. Opt. Soc. Am. A, vol.15, no 7, 1998.
[6] T. Martin, A. Koch, J. Synchrotron Rad. 13, 180-194, 2006.
[7] A. Cecilia et al., Journal Radiation Effects & Defects in Solids vol. 164 (9), p. 517–522 (2009).
[8] Rack et al.,Nuclear Instruments and Methods in Physics Research B 267 (2009).
[9] T. Weitkamp, "Imaging and Tomography with High Resolution Using Coherent Hard Synchrotron Radiation", Cuvillier Verlag Gottingen, Grenoble 2002.
[10] U. Bonse and F. Busch, Prog. Biophys. Molec. Biol. vol 65, 133-169, 1996.
[11] A.N. Danilewsky et al., Nuclear Instruments and Methods in Physics Research B 199 (2003) 71–74.
[12] A. N. Danilewsky, A. Rack, J. Wittge, T. Weitkamp, R. Simon, H. Riesemeier, T. Baumbach, Nuclear Instruments and Methods in Physics Research B vol. 266 (9), pp. 2035-2040 (2008).
[13] ANKA Instrumentation Book – http://www.fzk.de/anka (last visit July 2008).
[14] http://www.esrf.eu/UsersAndScience/Experiments/MaterialsScience/ID15/